Accepted for publication in *Atmospheric Environment* (Feb. 6th, 2010)

Comparison of calculation models for wind-driven rain deposition on building facades

B. Blocken* [(a)], G. Dezsö [(b)], J. van Beeck [(b)], J. Carmeliet [(c,d)]

(a) Building Physics and Systems, Eindhoven University of Technology, P.O. box 513, 5600 MB Eindhoven, the Netherlands
(b) Environmental and Applied Fluid Dynamics Department, von Karman Institute for Fluid Dynamics, Waterloosesteenweg 72, 1640 Sint-Genesius-Rode, Belgium
(c) Chair of Building Physics, Swiss Federal Institute of Technology ETHZ, ETH-Hönggerberg, CH-8093 Zürich, Switzerland
(d) Laboratory for Building Technologies, Swiss Federal Laboratories for Materials Testing and Research, Empa, Überlandstrasse 129, CH-8600 Dübendorf, Switzerland

Abstract

Wind-driven rain (WDR) is an important factor in the dry and wet deposition of atmospheric pollutants on building facades. In the past, different calculation models for WDR deposition on building facades have been developed and progressively improved. Today, the models that are most advanced and most frequently used are the semi-empirical model in the ISO Standard for WDR assessment (ISO), the semi-empirical model by Straube and Burnett (SB) and the CFD model by Choi. This paper compares the three models by applying them to four idealized buildings under steady-state conditions of wind and rain. In each case, the reference wind direction is perpendicular to the windward facade. For the CFD model, validation of wind-flow patterns and WDR deposition fluxes was performed in earlier studies. The CFD results are therefore considered as the reference case and the performance of the two semi-empirical models is evaluated by comparison with the CFD results based on two criteria: (1) ability to model the wind-blocking effect on the WDR coefficient; and (2) ability to model the variation of the WDR coefficient with horizontal rainfall intensity R_h. It is shown that both the ISO and SB model, as opposed to the CFD model, can not reproduce the wind-blocking effect. The ISO model incorrectly provides WDR coefficients that are independent of R_h, while the SB model shows a dependency that is opposite to that by CFD. In addition, the SB model can provide very large overestimations of the WDR deposition fluxes at the top and side edges of buildings (up to more than a factor 5). The capabilities and deficiencies of the ISO and SB model, as identified in this paper, should be considered when applying these models for WDR deposition calculations. The results in this paper will be used for improvement and further development of these models.

Keywords: driving rain; atmospheric deposition; Computational Fluid Dynamics; numerical simulation; model intercomparison

1. Introduction

Wind-driven rain (WDR) is an important factor in the dry and wet deposition of atmospheric pollutants on building facades. The water layer on the facade enhances the surface collection efficiency for pollutants brought to the facade by wind (dry deposition). Wet deposition occurs either directly, by WDR deposition/impingement, or indirectly, by the relocation of earlier dry and/or wet depositions by rainwater that runs down along the facade. Rainwater is also an agent for most physico-chemical deterioration processes. As such, it is an important boundary condition for facade surface soiling and facade erosion (Camuffo et al., 1982; Camuffo, 1992; Etyemezian et al., 2000; Tang et al., 2004; Blocken and Carmeliet, 2004). To study these problems and to analyse remedial measures, accurate calculation methods for WDR deposition on building facades are required.

WDR is governed by a wide range of parameters: building geometry, position on the building facade, environment topography, wind speed, wind direction, horizontal rainfall intensity and raindrop-size distribution. It is very complex and characterised by a high spatial and temporal variability. Therefore, assessing WDR deposition on building facades is a difficult task. Three main categories of assessment methods exist: measurements, semi-empirical models and numerical simulation based on Computational Fluid Dynamics

* **Corresponding author**: Building Physics and Systems, Eindhoven University of Technology, P.O.Box 513, 5600 MB Eindhoven, the Netherlands. Tel.: +31 (0)40 247 2138, Fax +31 (0)40 243 8595
E-mail address: b.j.e.blocken@tue.nl

(CFD). The term "semi-empirical" refers to models with a theoretical basis and with coefficients that are – at least partly – determined from measurements. A general review of these methods was provided by Blocken and Carmeliet (2004). The disadvantages associated with WDR measurements have driven researchers to develop calculation models, which have been progressively improved throughout the years. Today, the models that are most advanced and most frequently used are the semi-empirical model in the ISO Standard for WDR assessment (ISO 2009), the semi-empirical model by Straube (1998) and Straube and Burnett (2000) and the CFD model by Choi (1991, 1993, 1994). These three models are referred to as ISO, SB and CFD, respectively. The theory and some of the capabilities and limitations of these models have been outlined in (Blocken and Carmeliet, 2010). The semi-empirical models are easy to use and can be applied very fast, and this type of models is therefore implemented in most numerical Heat-Air-Moisture (HAM) transfer models for building facade analysis. However, these models do not take all the influencing parameters of WDR into account, are based on several assumptions (Blocken and Carmeliet, 2010) and there is almost no information on their accuracy. The CFD model on the other hand take into account most of the influencing parameters and have been validated with measurement data in the past. However, the CFD model is significantly more complex and computationally expensive. It is therefore important to study the accuracy of the semi-empirical models, which can be done by comparative studies. In a previous study (Blocken and Carmeliet 2010), the ISO, SB and CFD model were compared based on model theory. However, to the knowledge of the authors, a comparison study of the performance of these models when applied for WDR assessment of buildings has not yet been performed.

In this paper, the three models are compared by application to four idealised, isolated building configurations (Fig. 1). Four choices are made to reduce the complexity and to allow clear conclusions to be made: (1) The building configurations are taken as simple as possible: isolated buildings without facade details, situated on uniformly rough, flat terrain with aerodynamic roughness length $z_0 = 0.03$ m; (2) A neutral atmospheric boundary layer; (3) Four different building configurations are selected that are representative of a wide range of existing buildings: a low-rise cubic building, a low-rise wide building, a high-rise wide building and a tower building; (4) Steady-state conditions are considered: the mean wind speed U_{10}, wind direction φ_{10}, horizontal rainfall intensity R_h and horizontal raindrop-size distribution $f_h(d)$ are constant. U_{10} and φ_{10} are the reference wind speed and wind direction at 10 m height in the undisturbed flow. R_h is the horizontal rainfall rate (i.e. the rain deposition rate on a horizontal surface in free-field conditions). In this study, φ_{10} is taken perpendicular to the windward facade. The quantity to be calculated is the WDR coefficient α, which will be defined in the next section.

For the CFD model, validation of simulated wind-flow patterns (Blocken et al., 2009) and WDR deposition fluxes was performed in earlier studies based on wind tunnel and field measurements (Blocken and Carmeliet, 2002; 2006; 2007; Tang and Davidson, 2004; Abuku et al., 2009; Briggen et al., 2009). These validation studies have shown that the CFD model can provide accurate results. The CFD simulations are therefore considered as the reference case and the performance of the two semi-empirical models is evaluated by comparison with these CFD results.

This paper contains seven sections. In section 2, the three WDR calculation models are briefly described. Section 3 focuses on the buildings and the surrounding terrain. In section 4, the three WDR models are applied and the results are compared in detail for two of the four buildings. The comparison of the model results based on two specific criteria, for all four buildings, is provided in section 5. Sections 6 (discussion) and 7 (conclusions) conclude the paper.

2. Wind-driven rain deposition models

The WDR deposition rate R_{wdr} by each of the models can be written as:

$$R_{wdr} = \alpha \cdot U_{10} \cdot R_h^{0.88} \cdot \cos\theta \quad (1)$$

where α is the WDR coefficient and θ is the angle – in a horizontal plane – between the wind direction and the normal to the facade. Depending on the model, different expressions for α have to be used (Blocken and Carmeliet, 2010).

For wind perpendicular to the facade ($\theta = 0°$), the WDR coefficient in the CFD model is:

$$\alpha = \frac{\eta \cdot R_h^{0.12}}{U_{10}} \quad (2)$$

where η is the catch ratio from the CFD simulation, which is defined as the ratio R_{wdr}/R_h. Earlier research has shown that η is in good approximation a linear function of U_{10}, except at facade positions that are sheltered by

horizontal projections such as roof overhangs or balconies (Blocken and Carmeliet, 2002; 2006; 2008), which is not the case in this study. Therefore, α can be considered independent of U_{10}. Both η and α are a function of R_h.

The WDR coefficient in the ISO model is:

$$\alpha = \frac{2}{9} \cdot C_R \cdot C_T \cdot O \cdot W \tag{3}$$

where C_R is the roughness coefficient, C_T the topography coefficient, O the obstruction factor and W the wall factor. C_R takes into account the change of mean wind speed at the site due to the height above the ground and the upstream roughness of the terrain. It is given by:

$$C_R(z) = K_R \ln\left(\frac{z}{z_0}\right) \qquad \text{for } z \geq z_{min} \tag{4}$$

$$C_R(z) = C_R(z_{min}) \qquad \text{for } z < z_{min} \tag{5}$$

where z is the height above ground, K_R the terrain factor, z_0 the aerodynamic roughness length and z_{min} a minimum height. Values for these parameters are provided in the Standard (ISO 2009). For example, for z_0 = 0.01 m: K_R = 0.17 and z_{min} = 2 m, and for z_0 = 0.05 m: K_R = 0.19 and z_{min} = 4 m. The topography coefficient takes into account the increase of mean wind speed over isolated hills and escarpments. The obstruction factor O takes into account the shelter of the wall by the nearest obstacle. The wall factor W is defined as the "*ratio of the quantity of water hitting a wall to the quantity passing through an equivalent unobstructed space"*, i.e. the ratio of WDR on the building to free-field WDR. It tries to take into account the type of the wall (height, roof overhang) and the variation of WDR across the surface of the wall. Wall factors for two of the six buildings in the ISO Standard are shown in Fig. 2a-b. Note that α in this model is independent of U_{10} and R_h.

The WDR coefficient in the SB model is:

$$\alpha = DRF \,.\, RAF \,.\, \left(\frac{z}{10}\right)^{\beta} \cdot R_h^{0.12} \tag{6}$$

where DRF is the driving rain function, RAF the rain admittance factor and β the power-law exponent. For z_0 = 0.03 m, β is about 0.15. The DRF is calculated as the inverse of the terminal velocity of fall V_t, given by the equation by Dingle and Lee (1972):

$$V_t(d) = -0.166033 + 4.91844\, d - 0.888016\, d^2 + 0.054888\, d^3 \leq 9.20 \text{ m/s} \tag{7}$$

where d is the raindrop diameter. Concerning the choice of d, Straube and Burnett (2000) suggest the median diameter from the raindrop spectrum by Best (1950):

$$\bar{d} = 1.105\, R_h^{0.232} \tag{8}$$

The factor RAF is introduced to convert the free-field WDR intensity to the WDR intensity on the building facade. Based on their own WDR measurements and on a literature review, Straube and Burnett provided values of the RAF in graphical form for three types of building geometries, two of which are shown in Fig. 2c-d. Note that the third type of building (not shown) is a building with roof overhang. Straube and Burnett (2000) claimed that these contours and values are relatively building-scale independent. The SB model provides minimum and/or maximum limits for α, resulting from the minimum and maximum limits for the RAF in Fig. 2c-d. In this model, α is independent of U_{10}, but it is a function of R_h by the DRF and by the factor $R_h^{0.12}$.

More detailed information on these models can be found in the original references and in the overview paper (Blocken and Carmeliet, 2010).

3. Buildings and surrounding terrain

The four buildings are shown in Fig. 1. The buildings are isolated and are placed on a large, grass-covered, uniformly rough and flat terrain with z_0 = 0.03 m (Wieringa 1992). They are not exactly the same as used in an earlier study of the wind-blocking effect on the WDR exposure of building facades (Blocken and Carmeliet, 2006). While the geometry of buildings A and D is taken from this study, the geometry of buildings B and C is

based on the building models tested in the wind tunnel for validation purposes (Blocken et al., 2009). Note that even for buildings A and D, results might be slightly different from those in (Blocken and Carmeliet, 2006), because in the present paper, the Reynolds Stress Model (RSM) (Launder et al., 1975) is used instead of the realizable k-ε model (Shih et al., 1995). In addition, the inlet and ground boundary conditions are slightly different and a better grid quality is used in the present paper, as explained in section 4. The preference for the RSM is based on earlier validation studies, which proved this model to be more accurate for wind-flow patterns upstream of buildings (Blocken et al., 2009).

4. Wind-driven rain model application

The WDR models are applied to calculate α across the windward facade of the four buildings, for U_{10} = 10 m/s, $\theta = 0°$ and for a wide range of horizontal rainfall intensities R_h: 0.1-1 mm/h in steps of 0.1 mm/h, 1-2 mm/h in steps of 0.2 mm/h, 2-10 mm/h in steps of 2 mm/h and 10-30 mm/h in steps of 5 mm/h. Only one reference wind speed (10 m/s) is considered, because for the buildings in this study and for each model, α is independent of U_{10}, as explained in section 2.

4.1. CFD wind-flow pattern and raindrop tracking

3D steady Reynolds-averaged Navier-Stokes (RANS) simulations with the commercial code Fluent 6.3.26 are performed for the four buildings in computational domains with a maximum blockage ratio of 1.4%. The blockage ratio is the ratio of the projected area of the building in the flow direction to the cross-section of the domain. The buildings are placed at a distance of 20H from the inlet and at 15H from the outlet of the domain. The upstream distance is significantly larger than 5H recommended by Franke et al. (2007) and Tominaga et al. (2008a) because the raindrops have to be injected in the domain at a sufficiently large distance upstream of the building to avoid an influence of the injection position on the results. The computational grids are hybrid grids with a mixture of hexahedral and prismatic cells. They were constructed using the surface grid extrusion procedure presented by van Hooff and Blocken (2010). Each grid is based on grid-sensitivity analysis for the mean velocity components upstream of the building, because only these data are used to calculate the raindrop trajectories. The number of cells (non-uniform distribution) along the building width, depth and height are: 15x15x15 for building A (total number of cells is 1.1×10^5), 30x12x15 for building B (total 1.5×10^5), 30x12x30 for building C (total 2.9×10^5) and 15x12x35 for building D (total 2.1×10^5). All cell faces on the building surfaces are rectangular. Closure is obtained by the RSM (Launder et al. 1975) with a linear pressure-strain model and wall-reflection effects (Gibson and Launder 1978, Launder 1989). The turbulence model equations can be found in the related references, the model constants used in this study are the default values in Fluent 6.3.26 (Fluent Inc., 2006): $C_{1\varepsilon} = 1.44$; $C_{2\varepsilon} = 1.92$; $C_\mu = 0.09$; $C_{1PS} = 1.8$; $C_{2PS} = 0.6$; $C_1'_{PS} = 0.5$; $C_2'_{PS} = 0.3$; $\sigma_k = 1$; $\sigma_\varepsilon = 1.3$. In the subscripts, PS refers to "pressure-strain".

The vertical inlet profiles of mean wind speed, turbulent kinetic energy and turbulence dissipation rate are those by Richards and Hoxey (1993), with $z_0 = 0.03$ m, $C_\mu = 0.09$ and friction velocity $u^* = 0.69$ m/s corresponding to U_{10} = 10 m/s. Turbulent kinetic energy is converted to Reynolds stresses assuming isotropic turbulence. This assumption was shown to be justified and to provide accurate results for the mean velocity components (Blocken et al. 2009). The sides and the top of the computational domain are modelled as slip walls (zero normal velocity and zero normal gradients of all variables). Strictly, a better option would be to specify fixed profiles at the top boundary (Blocken et al. 2007a), but mainly because of the height of the domain (>6H), no influence of the type of boundary condition on the WDR results was found. At the outlet, zero static pressure is specified. For the ground boundary condition, the standard wall functions by Launder and Spalding (1974) with roughness modifications by Cebeci and Bradshaw (1977) are used. To limit problems of horizontal inhomogeneity due to inconsistent CFD simulation of the atmospheric boundary layer (Franke et al. 2007, Blocken et al. 2007a, 2007b), the equivalent sand-grain roughness height k_S and the roughness constant C_S are determined from z_0 using the function derived for Fluent 6 (valid up to at least version 6.3): $k_S = 9.793 z_0 / C_S$ (Blocken et al. 2007a). Note that for fully rough walls, only the product $k_S C_S$ appears in the wall functions, and therefore only the value of the product and not of the individual parameters k_S and C_S is important. Fluent 6 (up to at least version 6.3) does not allow k_S to be larger than z_P, which is the distance between the centre point of the wall-adjacent cell and the wall. If the user implements a larger value, the code will automatically set it equal to z_P without warning. Therefore, in this study, k_S is taken equal to z_P (= 0.2 m) and C_S is calculated from the function mentioned above: $C_S = 1.47$. A user-defined function setting the value of the constant C_S is required because the Fluent 6.3 code does not allow it to exceed the interval [0;1] otherwise.

Pressure-velocity coupling is taken care of by the SIMPLE algorithm. Pressure interpolation is second order. Second order discretization schemes are used for both the convection and the viscous terms of the governing equations.

The calculation of the raindrop trajectories by Lagrangian particle tracking and the calculation of the catch ratio are performed with author-written program codes. The characteristics and settings of these simulations are identical to those in (Blocken and Carmeliet, 2006). Calculations of the raindrop motions are conducted for a range of raindrop diameters: 0.5-1.0 mm in steps of 0.1 mm, 1.0-2.0 mm in steps of 0.2 mm and 2.0-6.0 mm in steps of 1.0 mm. Note that the calculations of the wind-flow pattern and the raindrop motions are uncoupled, i.e. raindrop motions are calculated based on the mean wind-flow pattern, but no influence of raindrop motion on the mean wind-flow pattern is considered. Earlier validation studies showed this approach to be justified (Blocken and Carmeliet 2002, 2006, 2007). For each position at the building facade (resolution 0.05 x 0.05 m²) and for each raindrop diameter, the catch ratio η is determined, using the raindrop spectrum by Best (1950).

4.2. Application for low-rise wide building

The three calculation models are applied for the low-rise wide building (building B). In the ISO model, C_R is only specified for z_0 = 0.01, 0.05, 0.3 and 1 m. To obtain results for z_0 = 0.03 m in the present study, the ISO WDR coefficient is calculated as the average of the WDR coefficients for z_0 = 0.01 m and 0.05 m. C_T and O are equal to one, because the terrain is considered flat and without obstructions. The wall factor W is obtained from the information in the Standard, which is partly reproduced in Fig. 2a-b in the present paper. For the "two-storey building with flat roof", W = 0.2 for the lower, 0.4 for the middle and 0.5 for the upper part of the facade. Note that W only increases with height, and not along the width of the facade.

For the SB model, the DRF and its parameters (Eqs. 6-8) are given in Table 1. The DRF shows a strong dependence on R_h, while this is much less pronounced for the product $DRF.R_h^{0.12}$. The RAF data for the building with W >> H is chosen (Fig. 2c).

The CFD results are shown in Fig. 3 as contours of α across the windward facade. The distribution (wetting pattern) can be mainly explained by two physical aspects: (1) the sweeping of raindrops by the wind to the building edges, which causes higher α-values at these edges (Choi 1994, Blocken and Carmeliet 2002) and (2) the wind-blocking effect (Blocken and Carmeliet 2006), which will be explained later. For buildings such as building B, a detailed physical explanation of the wetting pattern (for the catch ratio η) is given in (Blocken and Carmeliet 2006). Fig. 3 shows that the maximum α occurs at the top corner, and that for the entire facade, α increases as R_h increases. The gradients are especially pronounced in the vertical direction and near the top of the facade.

Fig. 4 compares the results by each model, for three R_h values and along two vertical lines: in the middle and at the edge of the windward facade. The CFD results are somewhat larger at the edge than in the middle. The ISO results show no variation along the width of the facade and with R_h. The SB model results along the edge are on average higher than those in the middle, although the maximum values at the top of both lines are identical. The SB results at the top decrease with increasing R_h.

Comparing the results in Fig. 4 shows that:

(1) Apart from the middle line at R_h = 1 mm/h and the edge line at R_h = 30 mm/h, the ISO model provides a fairly good agreement, although it generally underestimates the values at the top;
(2) For R_h = 1 mm/h, the values at the top and along the edge line are considerably overestimated by the SB model. For R_h = 10 and 30 mm/h however, the SB model provides quite good results.

4.3. Application for the tower building

For the ISO model, the same procedure as in section 4.2 is followed. The wall factor W is taken from the "multi-storey building with flat roof" (Fig. 2b). For the SB model, the RAF data for the building with H >> W is chosen (Fig. 2d).

Fig. 5 shows the CFD results. The explanation of the wetting pattern for this type of building is given in (Blocken and Carmeliet 2006). The main observations are that α increases with increasing R_h and that the vertical gradients are highest near the top edge. The ISO results in Fig. 6 are invariable from middle to edge line and invariable with R_h. The SB results along the edge are on average much higher than those in the middle, although the maximum values at the top of both lines are identical. The SB results at the top of each line decrease with increasing R_h.

Comparing the results in Fig. 6 shows that:

(1) The ISO model provides a good agreement for some cases, although it provides overestimations in Fig. 6a, and underestimations for the upper part of the facade in Fig. 6d,e,f;
(2) The SB model strongly overestimates the values near the top of the middle line and along the entire edge line, for all three R_h values. The variation of α with height along the edge line is a power law, due to the fact that the RAF is constant along this line (see Eq. 6 and Fig. 2d).

4.4. Application for the two other buildings

In the interest of brevity, not all results for the two other buildings (A and C) are shown here. Fig. 7 only shows the CFD results for R_h = 1 mm/h. The large difference in the results between these two buildings is mainly caused by the wind-blocking effect, as explained in (Blocken and Carmeliet 2006) and also in the next section. The application of the ISO model for these buildings follows the same procedure as in sections 4.2 and 4.3. For the SB model, the procedure is less straightforward for these two buildings, because for buildings without roof overhang, this model only provides RAF data for facades with large aspect ratios (Fig. 2c-d): either H >> W, or W >> H. Therefore, strictly, the SB model cannot be applied for buildings A and C. Because in practice, this model is expected to be applied just as well for these types of buildings, it will also be applied here. Note however that these results cannot be used to judge the SB model, but only to judge the use of this model for applications outside its intended purpose. In this paper, the RAF data for the case W >> H is used for these two buildings, because these results provide the closest agreement with the CFD results.

5. Comparison based on two criteria

The previous section has shown a mixed image of model performance, with the ISO and SB model performing well for some buildings and/or positions on windward facades and R_h values, while providing less good results for others. In an attempt to provide a clear evaluation of model performance, two criteria that are directly linked to the behaviour of WDR deposition on building facades are applied: (1) the reproduction of the wind-blocking effect on the WDR exposure; and (2) the reproduction of the variation of the WDR coefficient with R_h.

5.1. Reproduction of the wind-blocking effect

For isolated buildings and for WDR, the term "wind-blocking effect" primarily refers to the upstream disturbance of the wind-flow pattern by the presence of the building and the associated decrease of the upstream streamwise wind-velocity component (wind-speed slow-down). As the streamwise wind speed decreases, so does the streamwise horizontal raindrop speed, which results in lower WDR intensities at the facade. The higher and the wider the building, the stronger this effect will be. Therefore, the wind-blocking effect also refers to decreased WDR exposure due to increased building dimensions (width and height). The wind-blocking effect for WDR has been demonstrated by CFD simulations, but has also been confirmed by full-scale measurements of WDR on different parts of a test building (Blocken and Carmeliet 2006).

Comparing the WDR deposition patterns in Fig. 3b, 5b and 7 (all for R_h = 1 mm/h) clearly shows the wind-blocking effect. The low-rise cubic building A presents the least obstruction to the flow field, and therefore has on average the highest α across the facade. The low-rise wide building B introduces a higher amount of wind-blocking, yielding lower α values especially at the lower part of the facade. The high-rise wide building C presents the largest obstruction to the wind flow. The large wind-blocking effect yields very low WDR coefficients at the lower part of the facade, which remains almost dry. Finally, the tower building D, although higher, is also much narrower, and the wind-blocking effect is present, although less pronounced as for building C. This physical phenomenon, which can be observed with the CFD model, should - ideally - also be reproduced by the two semi-empirical models.

Since the wind-blocking effect is related to both the width and the height of the windward facade of the building, it can be related to the building scaling length BSL:

$$\mathrm{BSL} = \left(B_L \, B_S^{\,2}\right)^{\frac{1}{3}} \tag{9}$$

where B_L is the larger and B_S the smaller dimension of the windward facade. This parameter was defined by Wilson (1989) for estimating dimensions of flow recirculation regions on building roofs. The values of the BSL for buildings A, B, C and D are 10.0 m, 19.8 m, 50.0 m and 31.7 m, respectively.

Fig. 8 shows the average WDR coefficient α_{avg} over the facade as a function of the BSL, for R_h = 1, 10 and 30 mm/h, for the four buildings and the three calculation models. The following observations are made:

(1) For the CFD model, α_{avg} decreases with increasing BSL, which is in accordance with the wind-blocking effect;

(2) The ISO model only shows a decrease of α_{avg} with increasing BSL from the two low-rise buildings to the two high-rise buildings. This indicates that α_{avg} is primarily governed by the height of the building, rather than by the combination of building width and height. Therefore the ISO model does not correctly reproduce the wind-blocking effect;

(3) The SB model shows the opposite trend as the CFD model. α_{avg} is significantly larger for the tower building than for the low-rise wide building. Also in the SB model, α_{avg} is clearly related to building height, rather than to both building width and height.

5.2. Reproduction of the variation with horizontal rainfall intensity

Fig. 9 displays the variation of α_{avg} with R_h. The following observations are made:

(1) The three models disagree about the variation of α_{avg} with R_h. While the CFD values increase monotonically with increasing R_h, the ISO values show no variation with R_h and the SB values decrease monotonically with increasing R_h. The SB model predicts the opposite trend as the CFD model. The differences in the trends between CFD, ISO and SB are most pronounced for low R_h;
(2) The ISO model significantly underestimates α_{avg} for building A, while it overestimates it for building C. Predictions for buildings B and D are better, except for low R_h;
(3) The SB model overestimates α_{avg} for buildings C and D. It provides better results for buildings A and B, although the band between the limits SBmin and SBmax is very wide.

6. Discussion

6.1. CFD as reference solution

The two semi-empirical models have been evaluated by comparison with the CFD results. While the latter are not exact, they are considered significantly more accurate than the results by the semi-empirical models. The reason is that the implementation of the influencing parameters of WDR is most pronounced in the CFD model, as discussed in (Blocken and Carmeliet, 2010). In addition, the validation study of CFD wind-flow patterns and WDR deposition patterns on buildings in previous papers has shown that the CFD model can provide accurate results. Note that in most previous validation studies, the turbulent dispersion of raindrops was neglected. Generally, this has been shown to be a valid assumption, except for the bottom part of high-rise buildings when the reference wind speed U_{10} is low, as shown in the validation study by Briggen et al. (2009). The reason is that in this case, the raindrop trajectories (without turbulent dispersion) are almost parallel to the bottom part of the windward facade, and do not always impinge on the facade. Turbulent dispersion in the streamwise direction can cause these raindrops to deviate from their "mean" trajectory and to hit the facade anyway. This means that, when including turbulent dispersion, more rain will impinge on the lower part of the facade in reality than calculated with the CFD model. This statement is corroborated by an earlier study by Lakehal et al. (1995) who found that turbulent dispersion is an important factor increasing WDR on vertical walls in cases with weak upstream wind flow, such as in a street canyon. In the present study, the reference wind speed U_{10} has been taken deliberately high (10 m/s) to avoid this effect.

The distribution of WDR on the windward facade of a building is determined by the wind-flow pattern upstream of this facade, because it is this part of the flow pattern that is traversed by the raindrops before they impinge on the facade. When turbulent dispersion is not included, the raindrop trajectories are calculated based only on the mean wind-flow pattern. It is known that steady RANS, as used in this paper, is not capable of modelling the inherently transient nature of separation, recirculation and vortex shedding in the wake, and that calculation results in these regions are deficient (Murakami 1993, Tominaga et al. 2008b). However, as demonstrated by the validation studies, steady RANS seems to be accurate enough for the calculation of mean wind speed upstream of the building facade.

6.2. Comparison based on variation of α across the facade

Comparing the three models for buildings B and D has shown a mixed image of model performance.

(1) The ISO model provides a quite fair representation of the qualitative increase of α with height, although the curvature of each (near-vertical) line segment in Figs. 4 and 6 is convex instead of concave. This is especially clear for the high-rise building. In addition, the transition between the zones is abrupt. The ISO model does not take the variation of α across the width of the facade into account;
(2) The SB model provides a minimum and a maximum threshold for α, as a result of the min. and max. values of the RAF in Figs. 2c-d. Apart from the top edge of the facades of both buildings, and the vertical edge of the facade of building D, the difference between these values is (very) large, which reduces the predictive capacity.
(3) The SB model provides significant overestimations along the top edge and the vertical edge of the building facades for R_h = 1 mm/h. For building D, however, overestimations also occur for the other R_h values, and, along the edge line, the lower limit value SBmin locally goes up to more than 5 times the values by CFD.

The results by the ISO model are clearly better. The differences between the ISO and SB model have to be caused by differences in the factors in the model equations: Eq. (3) and (6). However, for R_h = 1, 10 and 30 mm/h, the product DRF.$R_h^{0.12}$ is about equal to 2/9 = 0.222 (see Table 1). Furthermore, for z_0 = 0.03 m, C_R in Eq. (4-5) is about equal to $(z/10)^{\beta}$ in Eq. (6). Finally, C_T = 1 and O = 1. As a result, the most important reason for the large differences observed between both models for R_h = 1, 10 and 30 mm/h is the difference between W and RAF. The large differences between W and RAF along the top and especially along the vertical edge of the facade are seen by comparing the values in Fig. 2a-b with those in Fig. 2c-d. These differences are surprising, given the fact that W and RAF have exactly the same definition; they are both defined as the ratio of WDR intensity on the building to free-field WDR intensity. Comparing the ISO and SB model results with the CFD results shows that, especially for the building D, the RAF values at the top and along the vertical edge are clearly too high.

6.3. Comparison based on wind-blocking effect and variation with R_h

The wind-blocking effect refers to the decrease of the WDR exposure with increasing BSL. This implies that for example the value of α_{avg} for the facade does not only depend on building height, but also on building width. The CFD results clearly show this double dependence, while the ISO and SB model do not. The variation of α_{avg} in both semi-empirical models is primarily governed by the building height. Note that the SB model claims the existence of building-scale independence – to some extent – for the RAF values in Fig. 2c-d (Straube 1998, Straube and Burnett 2000). This however is opposite to the existence of the wind-blocking effect and its relation to the BSL. Comparing Fig. 7a and b with each other indicates that, at least for the situation with W ≈ H, there is no building-scale independence of RAF values.

The variation of α_{avg} with R_h is clearly present for the CFD model, and is most pronounced at low R_h (< 10 mm/h). The assumption of the ISO model that α is independent of R_h is not valid. The SB model on the other hand provides the opposite trend compared to the CFD results. This is attributed to the strong dependence of the DRF on R_h, although this is partly balanced by the factor $R_h^{0.12}$, as shown in Table 1. While the DRF has provided good results for free-field WDR estimates (Straube 1998, Straube and Burnett 2000), it seems however that its dependence on R_h cannot be readily extrapolated to WDR assessment on building facades.

6.4. Other parameters

The comparison in this paper has only focused on the parameters building geometry, position at the facade and horizontal rainfall intensity. No comparison has been made concerning the parameters environment topography, wind direction and raindrop-size distribution. However, the present comparison study is considered an important first step towards further comparison studies that could include these additional parameters.

7. Conclusions

Three calculation models for wind-driven rain (WDR) have been compared by application to four idealised, isolated building configurations. The models are the semi-empirical model in the ISO Standard (ISO), the semi-empirical model by Straube and Burnett (SB) and the CFD model by Choi. Each model has been used to determine the WDR coefficient α at the windward facades. The comparison has first been made for the low-rise wide building and the tower building separately, and in a second stage for all four buildings, by considering two criteria: reproduction of the wind-blocking effect of the building on its WDR exposure and the variation of the surface-averaged α with horizontal rainfall intensity R_h. The main conclusions of the comparison are:

(1) The CFD results have been used as the reference solution to evaluate the results by the ISO and the SB model. This is justified based on a series of earlier CFD validation studies.

(2) The ISO model is applicable for all four building configurations, while the SB model can strictly only be applied for those buildings with either W >> H or W << H. Because in practice, the SB model will be used for all building and facade configurations, this has also been done in the present paper. The main evaluation of the SB model however was performed for those buildings for which it is intended.

(3) In the SB model, the RAF values at the top edge and vertical edge of the facade are too large, and for low R_h the dependence of the DRF on R_h is too strong. This does not mean that the DRF is not a good measure for free-field WDR. It does mean however that this concept cannot be readily extrapolated for WDR assessment on building facades. This is confirmed by the opposite trend between the SB and the CFD results as a function of R_h.

(4) The wind-blocking effect is well reproduced by the CFD model, but not by the ISO and the SB model. This effect implies that both the building height and the building width strongly influence the WDR exposure of

the facade. In the ISO and SB model, only the building height is considered as an important parameter, while the influence of building width is neglected (in ISO) or negligible (in SB).

(5) The increase of α with increasing R_h is clearly shown by the CFD model. The ISO model does not predict this dependency, while the SB shows the opposite trend.

The capabilities and deficiencies of the ISO and SB model, as identified in this paper, should be considered when applying these models for WDR deposition calculations. It should be noted that these two models are without any doubt considered very valuable. It is an admirable fact that these models were developed based on theoretical considerations and measurements only. They provide a strong and necessary basis for further model development, which can be guided by – among others – validated CFD simulations. The results in this paper will therefore be used to improve and further develop the semi-empirical models.

Acknowledgements

The authors thank the anonymous reviewers for very thoroughly reading this paper and for providing very valuable comments.

References

Abuku M., Blocken B., Nore K., Thue J.V., Carmeliet J., Roels S., 2009. On the validity of numerical wind-driven rain simulation on a rectangular low-rise building under various oblique winds. Building and Environment 44(3), 621– 632.

Best A.C., 1950. The size distribution of raindrops. Quarterly Journal of the Royal Meteorological Society 76, 16-36.

Blocken B., Carmeliet J., 2002. Spatial and temporal distribution of driving rain on a low-rise building. Wind and Structures 5(5), 441-462.

Blocken B., Carmeliet J., 2004. A review of wind-driven rain research in building science. Journal of Wind Engineering and Industrial Aerodynamics 92(13), 1079-1130.

Blocken B., Carmeliet J., 2006. The influence of the wind-blocking effect by a building on its wind-driven rain exposure. Journal of Wind Engineering and Industrial Aerodynamics 94(2), 101-127.

Blocken B., Carmeliet J., 2007. Validation of CFD simulations of wind-driven rain on a low-rise building facade. Building and Environment 42(7), 2530–2548.

Blocken B., Stathopoulos T., Carmeliet, J., 2007a. CFD simulation of the atmospheric boundary layer: wall function problems. Atmospheric Environment 41(2), 238-252.

Blocken B., Carmeliet J., Stathopoulos T., 2007b. CFD evaluation of the wind speed conditions in passages between buildings – effect of wall-function roughness modifications on the atmospheric boundary layer flow. Journal of Wind Engineering and Industrial Aerodynamics 95(9-11), 941-962.

Blocken B., Carmeliet J., 2008. Guidelines for the required time resolution of meteorological input data for wind-driven rain calculations on buildings. Journal of Wind Engineering and Industrial Aerodynamics 96(5), 621-639.

Blocken B., Carmeliet J., 2010. Overview of three state-of-the-art wind-driven rain assessment models and comparison based on model theory. Building and Environment 45(3), 691-703.

Blocken B., Dezsö G., van Beeck J., Carmeliet J., 2009. The mutual influence of two buildings on their wind-driven rain exposure and comments on the obstruction factor. Journal of Wind Engineering and Industrial Aerodynamics 97(5-6), 180-196.

Briggen P.M., Blocken. B, Schellen H.L., 2009. Wind-driven rain on the facade of a monumental tower: numerical simulation, full-scale validation and sensitivity analysis. Building and Environment 44(8), 1675–1690.

Camuffo D., Del Monte M., Sabbioni C., Vittori O., 1982. Wetting, deterioration and visual features of stone surfaces in an urban area. Atmospheric Environment 16(9), 2253-2259.

Camuffo D., 1992. Acid rain and deterioration of monuments: how old is the phenomenon? Atmospheric Environment 26B(2), 241-247.

Cebeci T., Bradshaw P., 1977. Momentum transfer in boundary layers. Hemisphere Publishing Corporation, New York.

Choi E.C.C., 1991. Numerical simulation of wind-driven-rain falling onto a 2-D building. Proceedings of Asia Pacific Conference on Computational Mechanics, Hong Kong, 1721-1728.

Choi, E.C.C., 1993. Simulation of wind-driven rain around a building. Journal of Wind Engineering and Industrial Aerodynamics 46&47, 721-729.

Choi, E.C.C., 1994. Determination of wind-driven rain intensity on building faces. Journal of Wind Engineering and Industrial Aerodynamics 51, 55-69.
Dingle A.N., Lee Y., 1972. Terminal fall speeds of raindrops. Journal of Applied Meteorology 11, 877-879.
Etyemezian V., Davidson C.I., Zufall M., Dai W., Finger S., Striegel M., 2000. Impingement of rain drops on a tall building. Atmospheric Environment 34, 2399-2412.
Fluent Inc., 2006. Fluent 6.3 user's guide, Lebanon.
Franke J., Hellsten A., Schlünzen H., Carissimo B., 2007. Best practice guideline for the CFD simulation of flows in the urban environment. COST Action 732: Quality Assurance and Improvement of Microscale Meteorological Models.
Gibson M.M., Launder B.E., 1978. Ground effects on pressure fluctuations in the Atmospheric Boundary Layer. Journal of Fluid Mechanics 86, 491-511.
ISO, 2009. Hygrothermal performance of buildings – Calculation and presentation of climatic data – Part 3: Calculation of a driving rain index for vertical surfaces from hourly wind and rain data. ISO 15927-3:2009 International Organization for Standardization.
Lakehal D., Mestayer P.G., Edson J.B., Anquetin S., Sini JF., 1995. Eulero-Lagrangian simulation of raindrop trajectories and impacts within the urban canopy. Atmospheric Environment 29(23), 3501–3517.
Launder B.E., 1989. Second-moment closure and its use in modeling turbulent industrial flows. International Journal of Numerical Methods in Fluids 9, 963-985.
Launder B.E., Reece G.J., Rodi W., 1975. Progress in the development of a Reynolds-stress turbulence closure. Journal of Fluid Mechanics 86, 537-566.
Launder B.E., Spalding D.B., 1974. The numerical computation of turbulent flows. Computer Methods in Applied Mechanics and Engineering 3, 269-289.
Murakami S., 1993. Comparison of various turbulence models applied to a bluff body. Journal of Wind Engineering and Industrial Aerodynamics 46 & 47, 21-36.
Richards P.J., Hoxey R.P., 1993. Appropriate boundary conditions for computational wind engineering models using the k-ε turbulence model. Journal of Wind Engineering and Industrial Aerodynamics 46&47, 145-153.
Shih T.H., Liou W.W., Shabbir A., Zhu J., 1995. A new k-ε eddy-viscosity model for high Reynolds number turbulent flows – model development and validation. Computers and Fluids 24, 3, 227-238.
Straube J.F., 1998. Moisture control and enclosure wall systems, Ph.D. thesis, Civil Engineering, University of Waterloo, Ontario, Canada, 318 p.
Straube J.F., Burnett E.F.P., 2000. Simplified prediction of driving rain on buildings. Proc. of the International Building Physics Conf., Eindhoven, The Netherlands, 18-21 September 2000, 375-382
Tang W., Davidson C.I., 2004. Erosion of limestone building surfaces caused by wind-driven rain. 2. Numerical modelling. Atmospheric Environment 38(33), 5601-5609.
Tominaga, Y., Mochida, A., Yoshie, R., Kataoka, H., Nozu, T., Yoshikawa, M., Shirasawa, T. 2008a. AIJ guidelines for practical applications of CFD to pedestrian wind environment around buildings. Journal of Wind Engineering and Industrial Aerodynamics 96(10-11) 1749-1761.
Tominaga Y., Mochida A., Murakami S., Sawaki S., 2008b. Comparison of various revised k–ε models and LES applied to flow around a high-rise building model with 1:1:2 shape placed within the surface boundary layer. Journal of Wind Engineering and Industrial Aerodynamics 96(4), 389-411.
van Hooff T., Blocken B., 2010. Coupled urban wind flow and indoor natural ventilation modelling on a high-resolution grid: a case study for the Amsterdam ArenA stadium. Environmental Modelling & Software 25(1), 51-65.
Wieringa J., 1992. Updating the Davenport roughness classification. Journal of Wind Engineering and Industrial Aerodynamics 41-44, 357-368.
Wilson D.J., 1989. Airflow around buildings, ASHRAE Handbook of Fundamentals, pp. 14.1-14.18.

Table 1. Calculation of driving rain function DRF and values of DRF versus $DRF.R_h^{0.12}$ in model by Straube and Burnett.

R_h (mm/h)	$\bar{d}$ (mm)	V_t (m/s)	DRF (s/m)	$R_h^{0.12}$ $(mm/h)^{0.12}$	$DRF.Rh^{0.12}$ $(s/m)(mm/h)^{0.12}$
1	1.11	4.26	0.235	1.000	0.235
10	1.89	6.32	0.158	1.318	0.209
30	2.74	7.77	0.136	1.504	0.205

FIGURES

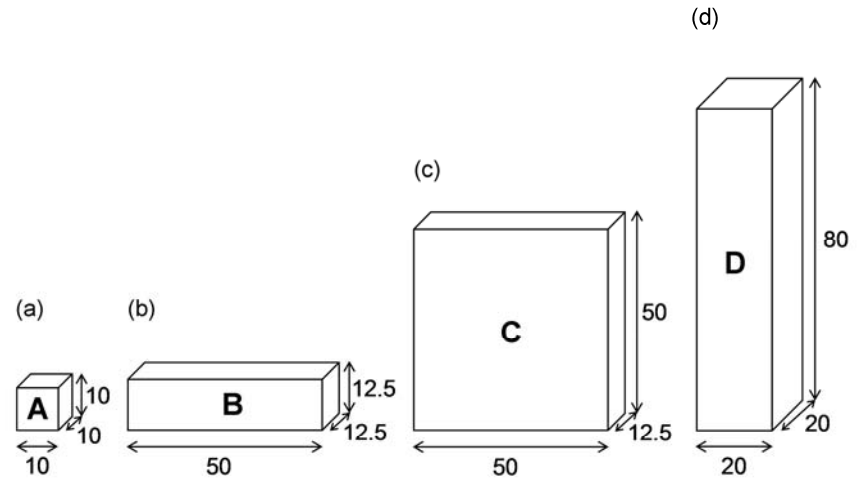

Fig. 1. Idealised building configurations: (a) low-rise cubic building A; (b) low-rise wide building B; (c) high-rise wide building C; (d) tower building D. Dimensions in m.

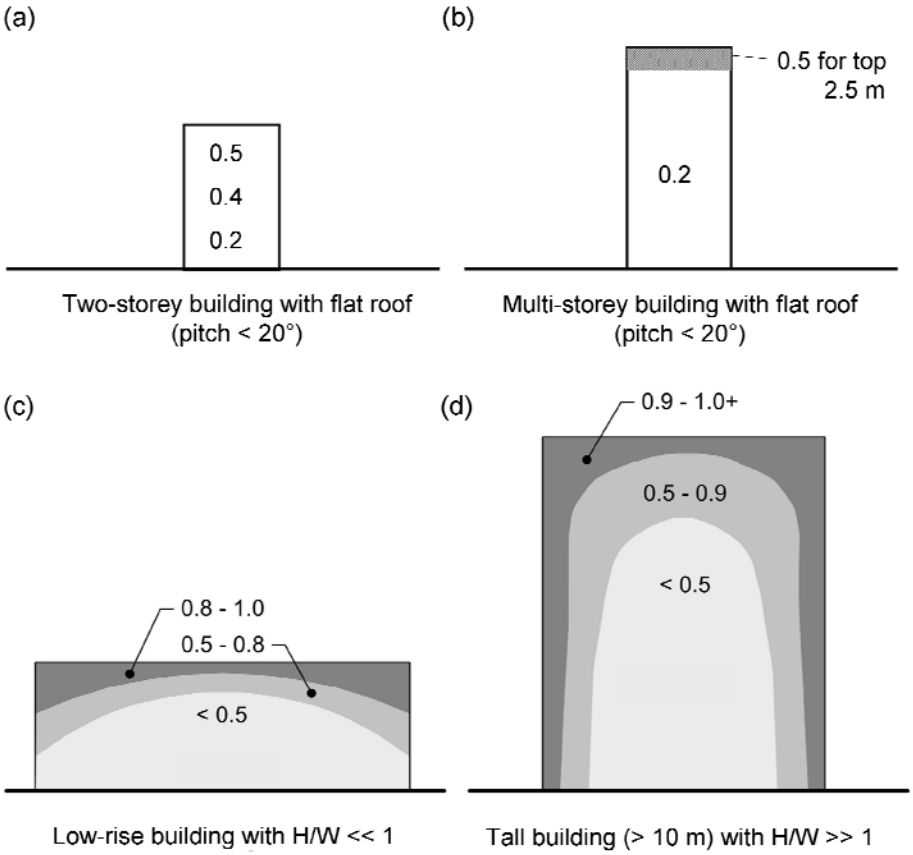

Fig. 2. (a-b) ISO Standard wall factors (W) on the windward facade of a two-storey building with flat roof and a multi-storey building with flat roof; (c-d) Contours of Straube and Burnett's rain admittance factor (RAF) on the windward facade of a low-rise and a high-rise building.

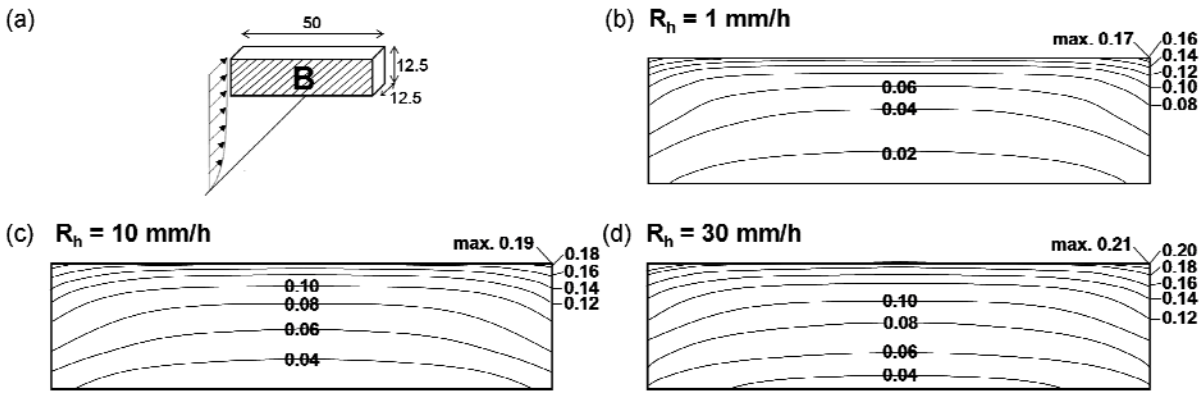

Fig. 3. Contours of wind-driven rain coefficient α (s/m) on the windward facade of the building B for three horizontal rainfall intensities R_h: (b) 1 mm/h; (c) 10 mm/h; (d) 30 mm/h.

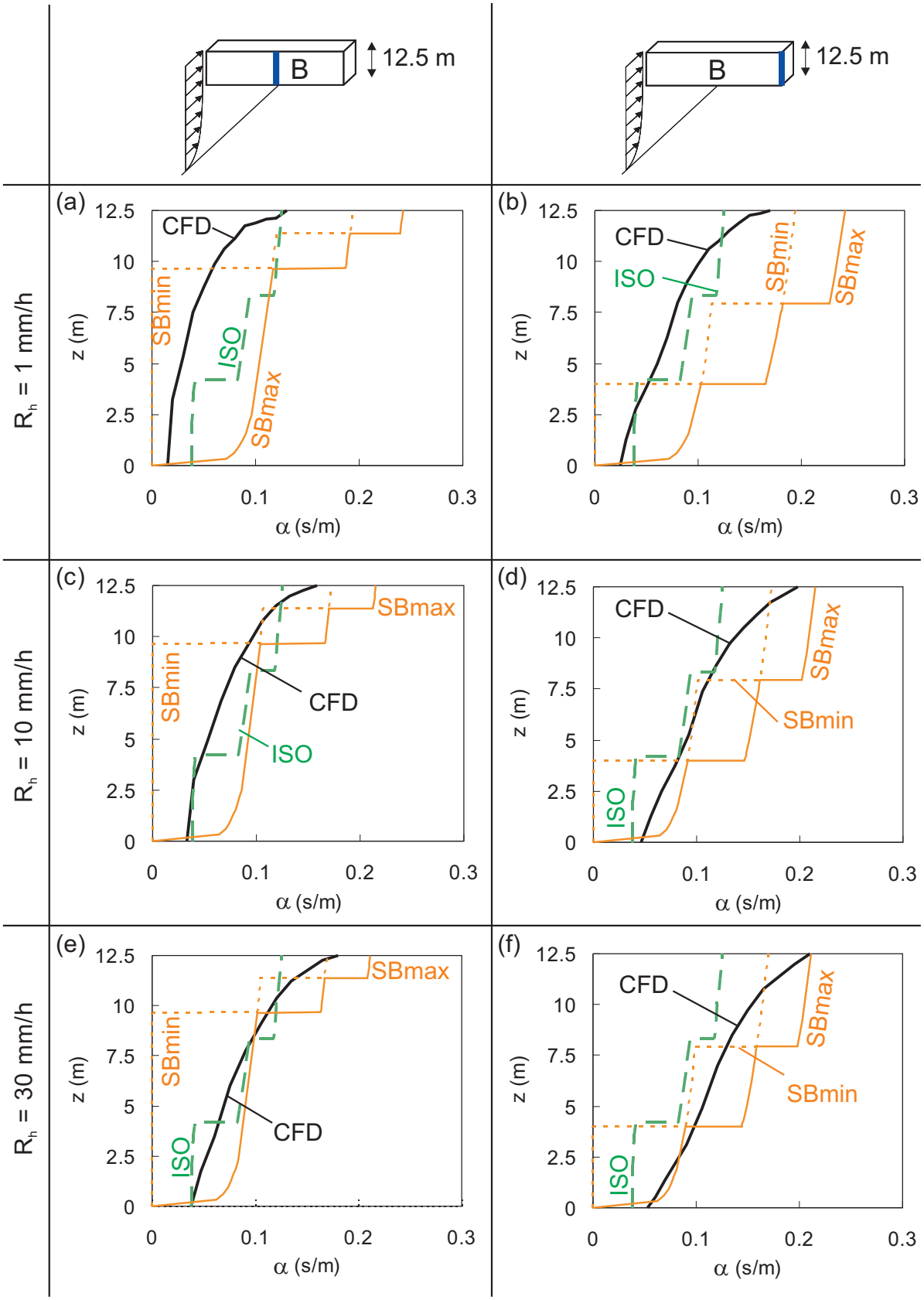

Fig. 4. Comparison of wind-driven rain coefficient α (s/m) for building B, as obtained by three models (CFD, ISO, SB) for three different horizontal rainfall intensities R_h (1, 10, 30 mm/h). The results are presented along two vertical lines: (a,c,e) middle and (b,d,f) edge.

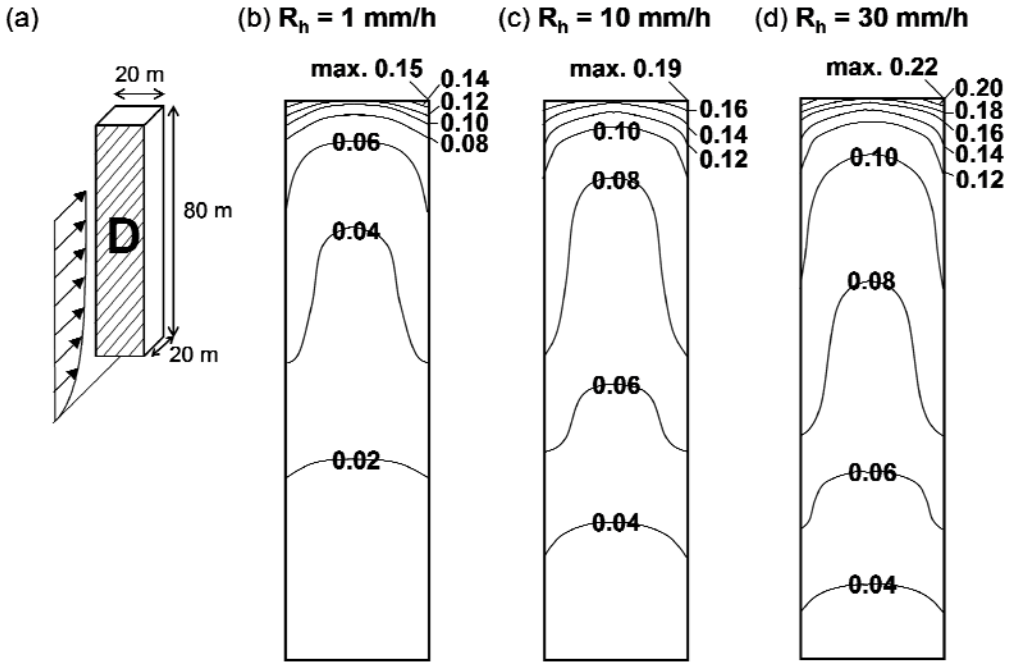

Fig. 5. Contours of wind-driven rain coefficient α (s/m) on the windward facade of building D for three horizontal rainfall intensities R_h: (b) 1 mm/h; (c) 10 mm/h; (d) 30 mm/h.

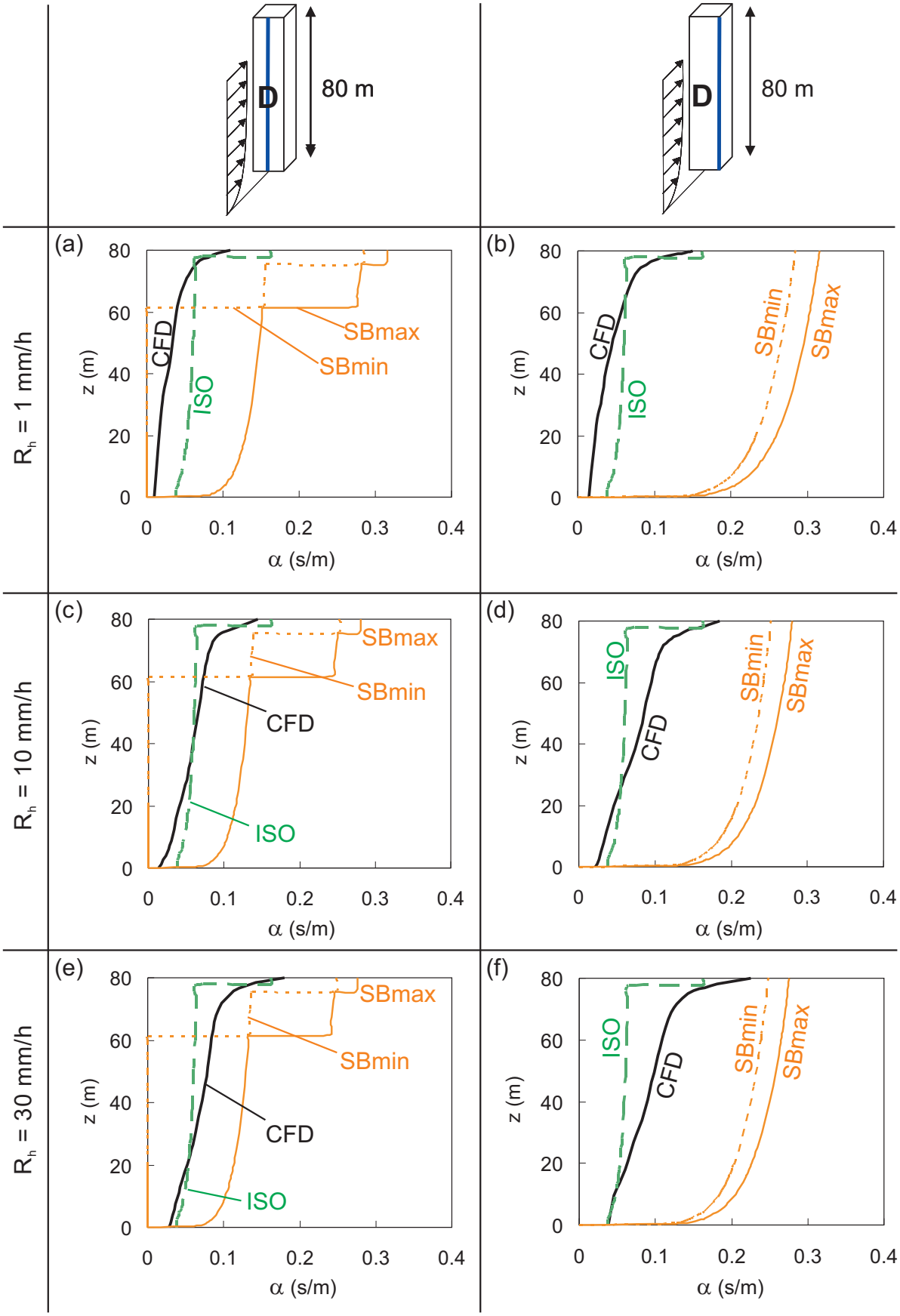

Fig. 6. Comparison of wind-driven rain coefficient α (s/m) for building D, as obtained by three models (CFD, ISO, SB) for three horizontal rainfall intensities R_h (1, 10, 30 mm/h). The results are presented along two vertical lines: (a,c,e) middle and (b,d,f) edge.

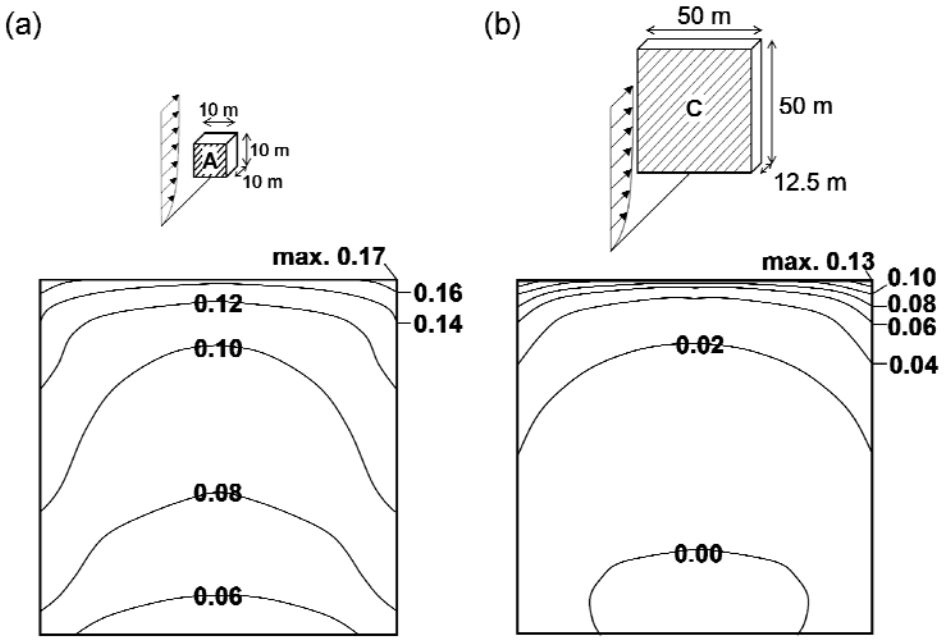

Fig. 7. Contours of wind-driven rain coefficient α (s/m) on the windward facade of buildings A and C, for R_h = 1 mm/h.

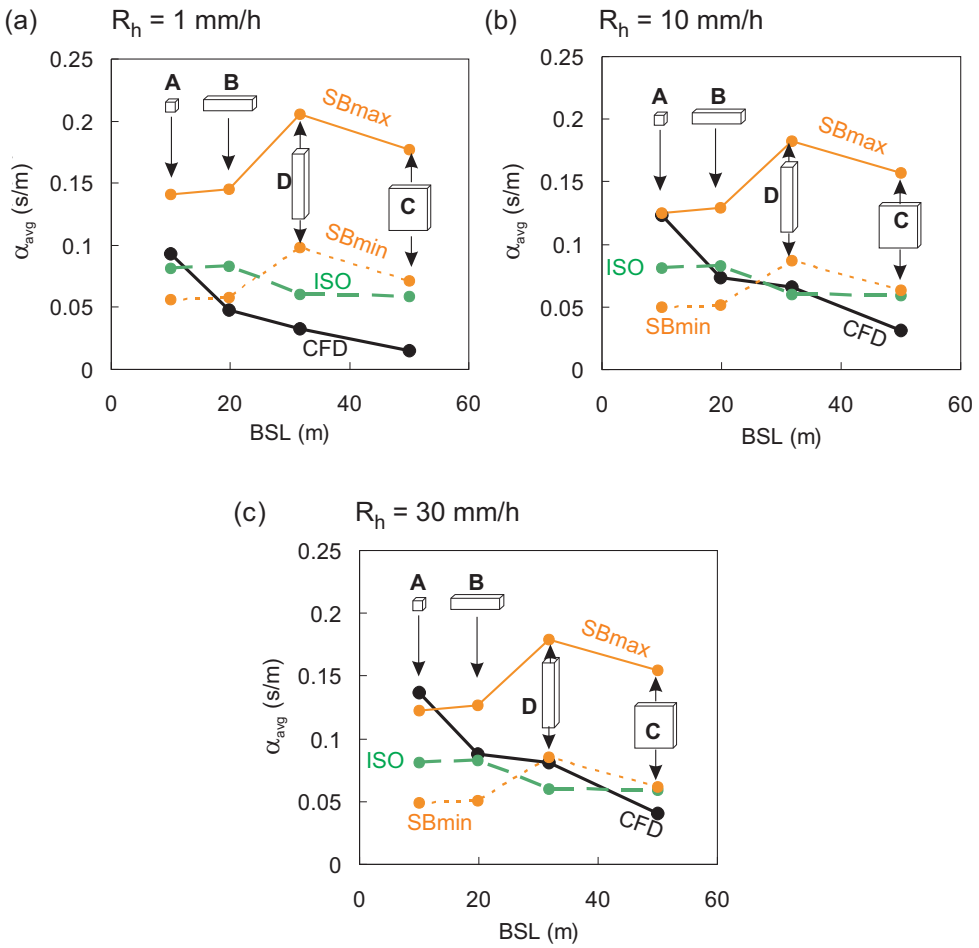

Fig. 8. Wind-driven rain coefficient averaged over the windward facade (α_{avg}) versus building scaling length (BSL), for the four buildings, the three calculation models and for three different horizontal rainfall intensities (a) R_h = 1 mm/h, (b) R_h = 10 mm/h and (c) R_h = 30 mm/h.

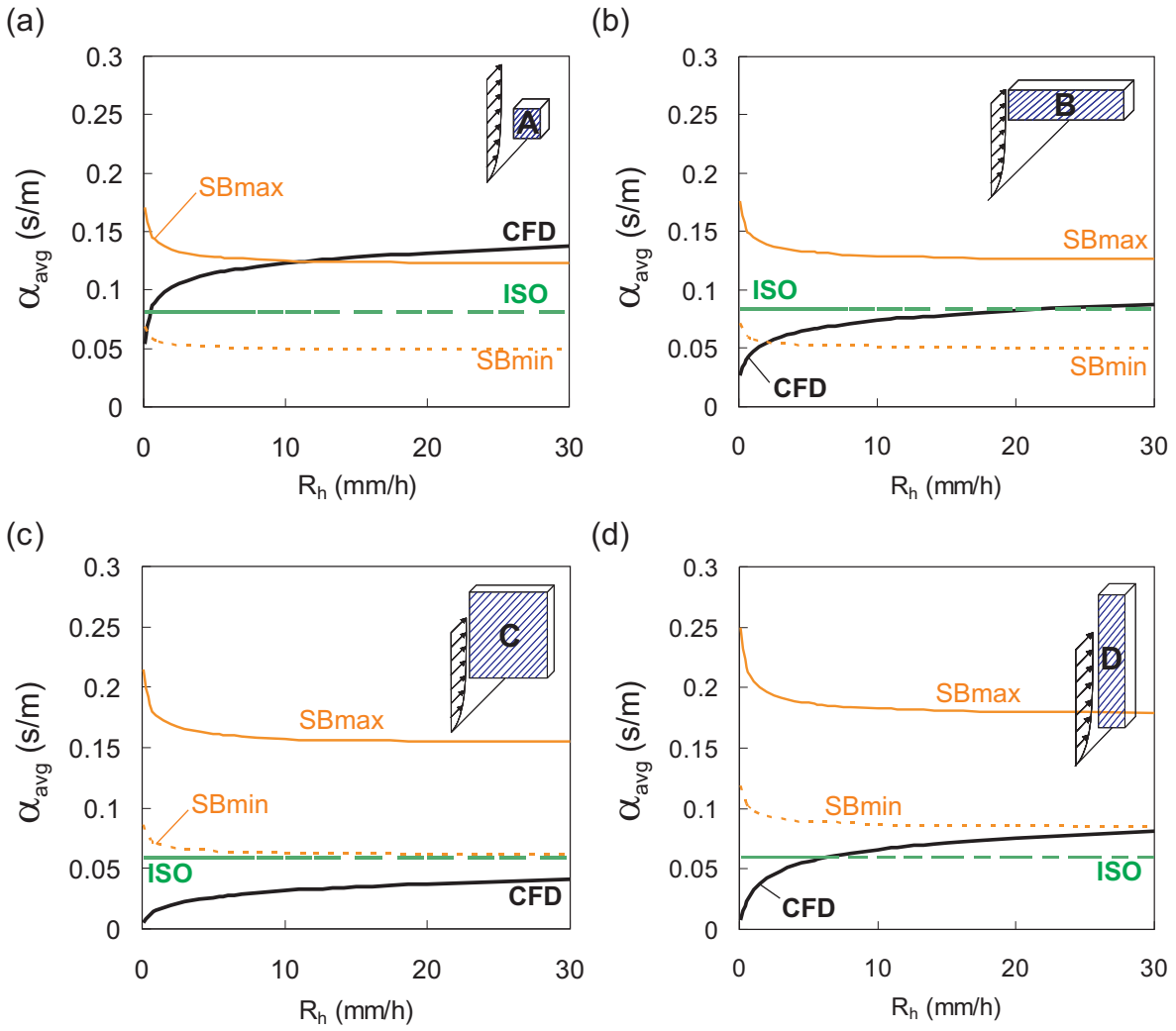

Fig. 9. Wind-driven rain coefficient averaged over the windward facade (α_{avg}) versus horizontal rainfall intensity R_h, for the four buildings and the three calculation models.